Informatik aktuell

Klaus Maier-Hein · Thomas M. Deserno
Heinz Handels · Andreas Maier
Christoph Palm · Thomas Tolxdorff *Hrsg.*

Bildverarbeitung für die Medizin 2022

Proceedings, German Workshop on Medical Image Computing, Heidelberg, June 26–28, 2022

Springer Vieweg

Informatik aktuell

Reihe herausgegeben von

Gesellschaft für Informatik e.V. (GI), Bonn, Deutschland

Ziel der Reihe ist die möglichst schnelle und weite Verbreitung neuer Forschungs- und Entwicklungsergebnisse, zusammenfassender Übersichtsberichte über den Stand eines Gebietes und von Materialien und Texten zur Weiterbildung. In erster Linie werden Tagungsberichte von Fachtagungen der Gesellschaft für Informatik veröffentlicht, die regelmäßig, oft in Zusammenarbeit mit anderen wissenschaftlichen Gesellschaften, von den Fachausschüssen der Gesellschaft für Informatik veranstaltet werden. Die Auswahl der Vorträge erfolgt im allgemeinen durch international zusammengesetzte Programmkomitees.

Weitere Bände in der Reihe https://link.springer.com/bookseries/2872

Klaus Maier-Hein · Thomas M. Deserno ·
Heinz Handels · Andreas Maier ·
Christoph Palm · Thomas Tolxdorff
(Hrsg.)

Bildverarbeitung für die Medizin 2022

Proceedings, German Workshop on Medical Image Computing, Heidelberg, June 26–28, 2022

Springer Vieweg

Hrsg.
Klaus Maier-Hein
Medical Image Computing, E230
Deutsches Krebsforschungszentrum (DKFZ)
Heidelberg, Deutschland

Heinz Handels
Institut für Medizinische Informatik
Universität zu Lübeck
Lübeck, Deutschland

Christoph Palm
Fakultät für Informatik und Mathematik
Ostbayerische Technische Hochschule Regensburg
Regensburg, Deutschland

Thomas M. Deserno
Peter L. Reichertz Institut für Medizinische Informatik der TU Braunschweig und der Medizinischen Hochschule Hannover
Braunschweig, Deutschland

Andreas Maier
Lehrstuhl für Mustererkennung
Friedrich-Alexander-Universität
Erlangen, Deutschland

Thomas Tolxdorff
Institut für Medizinische Informatik
Charité – Universitätsmedizin Berlin
Berlin, Deutschland

ISSN 1431-472X
Informatik aktuell
ISBN 978-3-658-36931-6 ISBN 978-3-658-36932-3 (eBook)
https://doi.org/10.1007/978-3-658-36932-3

Die Deutsche Nationalbibliothek verzeichnet diese Publikation in der Deutschen Nationalbibliografie; detaillierte bibliografische Daten sind im Internet über http://dnb.d-nb.de abrufbar.

© Der/die Herausgeber bzw. der/die Autor(en), exklusiv lizenziert durch Springer Fachmedien Wiesbaden GmbH, ein Teil von Springer Nature 2022
Das Werk einschließlich aller seiner Teile ist urheberrechtlich geschützt. Jede Verwertung, die nicht ausdrücklich vom Urheberrechtsgesetz zugelassen ist, bedarf der vorherigen Zustimmung des Verlags. Das gilt insbesondere für Vervielfältigungen, Bearbeitungen, Übersetzungen, Mikroverfilmungen und die Einspeicherung und Verarbeitung in elektronischen Systemen.
Die Wiedergabe von allgemein beschreibenden Bezeichnungen, Marken, Unternehmensnamen etc. in diesem Werk bedeutet nicht, dass diese frei durch jedermann benutzt werden dürfen. Die Berechtigung zur Benutzung unterliegt, auch ohne gesonderten Hinweis hierzu, den Regeln des Markenrechts. Die Rechte des jeweiligen Zeicheninhabers sind zu beachten.
Der Verlag, die Autoren und die Herausgeber gehen davon aus, dass die Angaben und Informationen in diesem Werk zum Zeitpunkt der Veröffentlichung vollständig und korrekt sind. Weder der Verlag, noch die Autoren oder die Herausgeber übernehmen, ausdrücklich oder implizit, Gewähr für den Inhalt des Werkes, etwaige Fehler oder Äußerungen. Der Verlag bleibt im Hinblick auf geografische Zuordnungen und Gebietsbezeichnungen in veröffentlichten Karten und Institutionsadressen neutral.

Planung: Petra Steinmüller
Springer Vieweg ist ein Imprint der eingetragenen Gesellschaft Springer Fachmedien Wiesbaden GmbH und ist ein Teil von Springer Nature.
Die Anschrift der Gesellschaft ist: Abraham-Lincoln-Str. 46, 65189 Wiesbaden, Germany

Bildverarbeitung für die Medizin 2022

Veranstalter

MIC	Medical Image Computing Deutsches Krebsforschungszentrum (DKFZ) Heidelberg

Unterstützende Fachgesellschaften

BVMI	Berufsverband Medizinischer Informatiker
CURAC	Computer- und Roboterassistierte Chirurgie
DAGM	Deutsche Arbeitsgemeinschaft für Mustererkennung
DGBMT	Fachgruppe Medizinische Informatik der Deutschen Gesellschaft für Biomedizinische Technik im Verband Deutscher Elektrotechniker
GI	Gesellschaft für Informatik – Fachbereich Informatik in den Lebenswissenschaften
GMDS	Gesellschaft für Medizinische Informatik, Biometrie und Epidemiologie
IEEE	Joint Chapter Engineering in Medicine and Biology, German Section

Tagungsvorsitz

Prof. Dr. Klaus H. Maier-Hein
Medical Image Computing (MIC)
Deutsches Krebsforschungszentrum (DKFZ), Heidelberg

Tagungssekretariat

Stefanie Strzysch, Theresa Klocke und Michaela Gelz
Medical Image Computing (MIC), DKFZ

Anschrift:	Im Neuenheimer Feld 223, 69120 Heidelberg
Email:	`orga-2022@bvm-workshop.org`
Web:	`https://bvm-workshop.org`

Lokale BVM-Organisation

Prof. Dr. Klaus Maier-Hein, Jasmin Metzger, Dr. Peter Neher, Dr. Beatrix Tettmann, Dr. Daniel Walther, Dimitrios Bounias, Dr. Kathrin Brunk, Maximilian Fischer, Philipp Schader, Shuhan Xiao, Silvia Dias Almeida, u.v.m.

Verteilte BVM-Organisation

Begutachtung	Heinz Handels und Jan-Hinrich Wrage – Institut für Medizinische Informatik, Universität zu Lübeck
Mailingliste	Klaus Maier-Hein – Medical Image Computing, Deutsches Krebsforschungszentrum (DKFZ) Heidelberg
Special Issue	Andreas Maier – Lehrstuhl für Mustererkennung, Friedrich-Alexander Universität Erlangen-Nürnberg
Sponsoring	Thomas Tolxdorff und Thorsten Schaaf – Institut für Medizinische Informatik, Charité-Universitätsmedizin Berlin
Tagungsband	Thomas M. Deserno, Michael Völcker, Nick Igelbrink und Nico Stautmeister – Peter L. Reichertz Institut für Medizinische Informatik (PLRI), Technische Universität Braunschweig und Medizinische Hochschule Hannover
Web & News	Christoph Palm, Leonard Klausmann, Alexander Leis und Sümeyye R. Yildiran – Regensburg Medical Image Computing (ReMIC), Ostbayerische Technische Hochschule Regensburg

BVM-Komitee

Prof. Dr. Thomas M. Deserno, Peter L. Reichertz Institut für Medizinische Informatik (PLRI), Technische Universität Braunschweig und Medizinische Hochschule Hannover

Prof. Dr. Heinz Handels, Institut für Medizinische Informatik, Universität zu Lübeck

Prof. Dr. Andreas Maier, Lehrstuhl für Mustererkennung, Friedrich-Alexander-Universität Erlangen-Nürnberg

Prof. Dr. Klaus Maier-Hein, Medical Image Computing, Deutsches Krebsforschungszentrum Heidelberg

Prof. Dr. Christoph Palm, Regensburg Medical Image Computing (ReMIC), Ostbayerische Technische Hochschule Regensburg

Prof. Dr. Thomas Tolxdorff, Institut für Medizinische Informatik, Charité–Universitätsmedizin Berlin

Programmkomitee

Jürgen Braun, Charité-Universitätsmedizin Berlin
Thomas M. Deserno, TU Braunschweig
Jan Ehrhardt, Universität zu Lübeck
Sandy Engelhardt, Universitätsklinik Heidelberg
Ralf Floca, DKFZ Heidelberg
Nils Forkert, University of Calgary, Canada
Michael Götz, Universitätsklinikum Ulm
Horst Hahn, Fraunhofer MEVIS, Bremen
Heinz Handels, Universität zu Lübeck
Tobias Heimann, Siemens Healthcare, Erlangen
Mattias Heinrich, Universität zu Lübeck
Anja Hennemuth, Charité-Universitätsmedizin Berlin
Alexander Horsch, The Arctic University of Norway, Tromsø, Norwegen
Dagmar Kainmüller, MDC Berlin
Ron Kikinis, Harvard Medical School, Boston, USA
Dagmar Krefting, Universität Göttingen
Andreas Maier, Universität Erlangen-Nürnberg
Klaus Maier-Hein, DKFZ Heidelberg
Lena Maier-Hein, DKFZ Heidelberg
Andre Mastmeyer, Hochschule Aalen
Dorit Merhof, RWTH Aachen
Jan Modersitzki, Fraunhofer MEVIS, Lübeck
Heinrich Müller, TU Dortmund
Nassir Navab, TU München
Marco Nolden, DKFZ Heidelberg
Christoph Palm, OTH Regensburg
Bernhard Preim, Universität Magdeburg
Stefanie Remmele, HAW Landshut
Petra Ritter, BIH Berlin
Karl Rohr, Universität Heidelberg
Daniel Rückert, TU München
Sylvia Saalfeld, Universität Magdeburg
Dennis Säring, FH Wedel
Julia Schnabel, TU München/Helmholtz Zentrum München
Ingrid Scholl, FH Aachen
Stefanie Speidel, HZDR (NCT Dresden)
Thomas Tolxdorff, Charité-Universitätsmedizin Berlin
Klaus Tönnies, Universität Magdeburg
Gudrun Wagenknecht, Forschungszentrum Jülich
René Werner, UKE Hamburg
Thomas Wittenberg, Fraunhofer IIS Erlangen
Ivo Wolf, Hochschule Mannheim

Preisträger der BVM 2021 in Regensburg

Beste wissenschaftliche Arbeiten

1. **Tristan M. Gottschalk**
   (Lehrstuhl für Mustererkennung, Friedrich-Alexander Universität Erlangen-Nürnberg)
   Gottschalk TM, Maier A, Kordon F, Kreher BW
   Learning-Based Patch-Wise Metal Segmentation with Consistency Check

1. **Jan Macdonald**
   (Institut für Mathematik, Technische Universität Berlin)
   Macdonald J, März M, Oala L, Samek W
   Interval Neural Networks as Instability Detectors for Image Reconstructions

3. **Alexander Bigalke**
   (Institut für Medizinische Informatik, Universität zu Lübeck)
   Bigalke A, Hansen L, Heinrich MP
   End-to-end learning of body weight prediction from point clouds with basis point sets

Bester Vortrag

Katharina Breininger
(Lehrstuhl für Mustererkennung, Friedrich-Alexander-Universität Erlangen-Nürnberg)
Breininger K, Pfister M, Kowarschik M, Maier A
Move Over There: One-click Deformation Correction for Image Fusion During Endovascular Aortic Repair

Bestes Poster

Carina Tschigor
(Frauenhofer MEVIS, Bremen)
Tschigor C, Chlebus G, Schumann C
Deep Learning-basierte Oberflächenrekonstruktion aus Binärmasken

Vorwort

Die Tagung *Bildverarbeitung für die Medizin (BVM)* wird seit weit mehr als 20 Jahren an wechselnden Orten Deutschlands veranstaltet. Inhaltlich fokussiert sich die BVM dabei auf die computergestützte Analyse medizinischer Bilddaten mit vielfältigen Anwendungsgebieten, z.B. im Bereich der Bildgebung, der Diagnostik, der Operationsplanung, der computerunterstützten Intervention und der Visualisierung.

In dieser Zeit hat es bemerkenswerte methodische Weiterentwicklungen und Umbrüche gegeben, wie zum Beispiel im Bereich des maschinellen Lernens, an denen die BVM-Community intensiv mitgearbeitet hat. In der Folge dominieren inzwischen Arbeiten im Zusammenhang mit *Deep Learning* die BVM. Auch diese Entwicklungen haben dazu beigetragen, dass die Medizinische Bildverarbeitung an der Schnittstelle zwischen Informatik und Medizin als eine der Schlüsseltechnologien zur Digitalisierung des Gesundheitswesens etabliert ist.

Zentraler Aspekt der BVM ist neben der Darstellung aktueller Forschungsergebnisse schwerpunktmäßig aus der vielfältigen deutschlandweiten BVM-Community insbesondere die Förderung des wissenschaftlichen Nachwuchses. Die Tagung dient vor allem Doktorand*innen und Postdoktorand*innen, aber auch Studierenden mit hervorragenden Bachelor- und Masterarbeiten als Plattform, um ihre Arbeiten zu präsentieren, dabei in den fachlichen Diskurs mit der Community zu treten und Netzwerke mit Fachkolleg*innen zu knüpfen. Trotz der vielen Tagungen und Kongresse, die auch für die Medizinische Bildverarbeitung relevant sind, hat die BVM deshalb nichts von ihrer Bedeutung und Anziehungskraft eingebüßt.

Inhaltlich kann auch bei der BVM 2022 wieder ein attraktives und hochklassiges Programm geboten werden. Es wurden aus 88 Einreichungen über ein anonymisiertes Reviewing-Verfahren mit jeweils drei Reviews 24 Vorträge, 33 Posterbeiträge und eine Softwaredemonstration angenommen. Da aufgrund der strengen Covid Hygiene- und Abstandsregeln leider nur sehr wenige klassische Posterbeiträge zugelassen wurden, wird dieses Jahr erstmalig ein neues Format umgesetzt. Hierfür wurden 13 weitere Beiträge als e-Poster angenommen. Die besten Arbeiten werden auch in diesem Jahr mit Preisen ausgezeichnet. Die Webseite des Workshops findet sich unter `https://www.bvm-workshop.org`.

Das Programm wird durch drei eingeladene Vorträge ergänzt:

- **Prof. Dr. Ullrich Köthe**, Visual Learning Lab, Universität Heidelberg
- **Prof. Mihaela van der Schaar**, University of Cambridge, UK
- **Prof. Dr. Stefanie Speidel**, Translational Surgical Oncology, NCT Dresden

Des Weiteren werden im Vorfeld der BVM drei Tutorials angeboten:

- **Known Operator Learning and Hybrid Machine Learning in Medical Imaging The Past, the Present and the Future** (FAU Erlangen-Nürnberg)
- **Advanced Deep Learning** (DKFZ Heidelberg)
- **Hands-On Medical Image Registration** (Universität zu Lübeck)

An dieser Stelle möchten wir allen, die bei den umfangreichen Vorbereitungen zum Gelingen des Workshops beigetragen haben, unseren herzlichen Dank für ihr Engagement aussprechen: den Referent*innen der Gastvorträge, den Autor*innen der Beiträge, den Referent*innen der Tutorien, den Industrierepräsentant*innen, dem Programmkomitee, den Fachgesellschaften, den Mitgliedern des BVM-Organisationsteams und allen Mitarbeitenden der Abteilung Medical Image Computing des Deutschen Krebsforschungszentrums.

Wir wünschen allen Teilnehmer*innen des Workshops BVM 2022 spannende neue Kontakte und inspirierende Eindrücke aus der Welt der medizinischen Bildverarbeitung.

Januar 2022

Klaus Maier-Hein (Heidelberg)
Thomas M. Deserno (Braunschweig)
Heinz Handels (Lübeck)
Andreas Maier (Erlangen)
Christoph Palm (Regensburg)
Thomas Tolxdorff (Berlin)

Inhaltsverzeichnis

Die fortlaufende Nummer am linken Seitenrand entspricht den Beitragsnummern, wie sie im endgültigen Programm des Workshops zu finden sind. Dabei steht V für Vortrag, P für Poster, E für ePoster und S für Softwaredemonstration.

Session 1: Segmentation I

V1 *Julia Andresen, Timo Kepp, Michael Wang-Evers, Jan Ehrhardt, Dieter Manstein, Heinz Handels*
Unsupervised Segmentation of Wounds in Optical Coherence Tomography Images Using Invariant Information Clustering 1

V2 *Mona Schumacher, Ragnar Bade, Andreas Genz, Mattias Heinrich*
Iterative 3D CNN Based Segmentation of Vascular Trees in Liver CT 7

V3 *Annika Hänsch, Felix Thielke, Hans Meine, Shereen Rennebaum, Matthias F. Froelich, Lena S. Becker, Jan B. Hinrichs, Andrea Schenk*
Robust Liver Segmentation with Deep Learning Across DCE-MRI Contrast Phases 13

V4 *Hellena Hempe, Mattias P. Heinrich*
Abstract: Light-weight Semantic Segmentation and Labelling of Vertebrae in 3D-CT Scans 19

Session 2: Segmentation II

V5 *Mingxuan Gu, Sulaiman Vesal, Ronak Kosti, Andreas Maier*
Few-shot Unsupervised Domain Adaptation for Multi-modal Cardiac Image Segmentation 20

V6 *David Zimmerer, Daniel Paech, Carsten Lüth, Jens Petersen, Gregor Köhler, Klaus Maier-Hein*
Unsupervised Anomaly Detection in the Wild 26

V7 *Timo Kepp, Julia Andresen, Helge Sudkamp, Claus von der Burchard, Johann Roider, Gereon Hüttmann, Jan Ehrhardt, Heinz Handels*
Epistemic and Aleatoric Uncertainty Estimation for PED Segmentation in Home OCT Images 32

V8 *Camila González, Christian L. Harder, Amin Ranem, Ricarda Fischbach, Isabel J. Kaltenborn, Armin Dadras, Andreas M. Bucher, Anirban Mukhopadhyay*
Quality Monitoring of Federated Covid-19 Lesion Segmentation 38

Session 3: Detection

V9 *Florian Thamm, Oliver Taubmann, Markus Jürgens, Hendrik Ditt, Andreas Maier*
Detection of Large Vessel Occlusions Using Deep Learning by Deforming Vessel Tree Segmentations 44

V10 *Michael Baumgartner, Paul F. Jäger, Fabian Isensee, Klaus H. Maier-Hein*
Abstract: nnDetection: A Self-configuring Method for Medical Object Detection 50

V11 *Disha D. Rao, Nicole Maass, Frank Dennerlein, Andreas Maier, Yixing Huang*
Machine Learning-based Detection of Spherical Markers in CT Volumes 51

V12 *Aline Sindel, Bettina Hohberger, Sebastian Fassihi Dehcordi, Christian Mardin, Robert Lämmer, Andreas Maier, Vincent Christlein*
A Keypoint Detection and Description Network Based on the Vessel Structure for Multi-modal Retinal Image Registration 57

Session 4: Registration / Detection

V13 *Richin Sukesh, Andreas Fieselmann, Srikrishna Jaganathan, Karthik Shetty, Rainer Kärgel, Florian Kordon, Steffen Kappler, Andreas Maier*
Training Deep Learning Models for 2D Spine X-rays Using Synthetic Images and Annotations Created from 3D CT Volumes 63

V14 *Stephanie Häger, Annkristin Lange, Stefan Heldmann, Jan Modersitzki, Andreas Petersik, Manuel Schröder, Heiko Gottschling, Thomas Lieth, Erich Zähringer, Jan H. Moltz*
Robust Intensity-based Initialization for 2D-3D Pelvis Registration (RobIn) 69

V15 *Fenja Falta, Lasse Hansen, Marian Himstedt, Mattias P. Heinrich*
Learning an Airway Atlas from Lung CT Using Semantic Interpatient Deformable Registration 75

V16 *Hristina Uzunova, Heinz Handels, Jan Ehrhardt*
Abstract: Guided Filter Regularization for Improved Disentanglement of Shape and Appearance in Diffeomorphic Autoencoders 81

Session 5: Surgical Data Science / Virtual Reality

V17 *Florian Kordon, Andreas Maier, Benedict Swartman, Maxim Privalov, Jan S. El Barbari, Holger Kunze*
Abstract: Automatic Path Planning for Safe Guide Pin Insertion in PCL Reconstruction Surgery 82

V18 *Jan Hombeck, Nils Lichtenberg, Kai Lawonn*
Heads up: A Study of Assistive Visualizations for Localisation Guidance in Virtual Reality 83

V19 *Niklas Hermes, Lasse Hansen, Alexander Bigalke, Mattias P. Heinrich*
Support Point Sets for Improving Contactless Interaction in Geometric Learning for Hand Pose Estimation 89

V20 *Arpitha Ravi, Florian Kordon, Andreas Maier*
Automatic Switching of Organ Programs in Interventional X-ray Machines Using Deep Learning 95

Session 6: Surgical Data Science / Simulation / Data Sets

V21 *Carina Krosse, Rainer Brucher, Alfred Franz*
Ermittlung der Geometrie von Amputationsstümpfen mittels Ultraschall 101

V22 *Fabian Wagner, Mareike Thies, Marek Karolczak, Sabrina Pechmann, Yixing Huang, Mingxuan Gu, Lasse Kling, Daniela Weidner, Oliver Aust, Georg Schett, Silke Christiansen, Andreas Maier*
Monte Carlo Dose Simulation for In-Vivo X-Ray Nanoscopy 107

V23 *Matthias Eisenmann, Minu D. Tizabi, Keno März, Lena Maier-Hein*
Abstract: How to Generate Patient Benefit with Surgical Data Science: Results of an International Delphi Process 113

V24 *Beatriz Garcia Santa Cruz, Matias Nicolas Bossa, Jan Soelter, Frank Hertel, Andreas Husch*
Abstract: The Importance of Dataset Choice: Lessons Learned from COVID-19 X-ray Imaging Models 114

Postersession 1

P1 *David Rauber, Robert Mendel, Markus W. Scheppach, Alanna Ebigbo, Helmut Messmann, Christoph Palm*
Analysis of Celiac Disease with Multimodal Deep Learning 115

P2 *Weilin Fu, Lennart Husvogt, Katharina Breininger, Roman Schaffert, Omar Abu-Qamar, James G. Fujimoto, Andreas Maier*
Form Follows Function: Smart Network Design Enables Zero-shot Network Reuse 121

P3 *Lisa Kausch, Sarina Thomas, Holger Kunze, Tobias Norajitra, André Klein, Jan El Barbari, Maxim Privalov, Sven Vetter, Andreas Mahnken, Lena Maier-Hein, Klaus Maier-Hein*
Abstract: C-arm Positioning for Spinal Standard Projections in Different Intra-operative Settings 127

P4 *Ivo M. Baltruschat, Hanna Ćwieka, Diana Krüger, Berit Zeller-Plumhoff, Frank Schlünzen, Regine Willumeit-Römer, Julian Moosmann, Philipp Heuser*
Abstract: Verbesserung des 2D U-Nets für die 3D Mikrotomographie mit Synchrotronstrahlung mittels Multi-Axes Fusing 128

P5 *Luisa Neubig, René Groh, Melda Kunduk, Deirdre Larsen, Rebecca Leonard, Andreas M. Kist*
Efficient Patient Orientation Detection in Videofluoroscopy Swallowing Studies 129

P6 *Nikolaus Arbogast, Holger Kunze, Florian Kordon, Benedict Swartman, Jan S. El Barbari, Katharina Breininger*
Towards Weakly Supervised Segmentation of Orthopaedic X-ray Images Using Constrained-CNN Losses 135

P7 *Ralf Hackner, Thomas Eixelberger, Milan Schmidle, Volker Bruns, Edgar Lehmann, Udo Geissler, Thomas Wittenberg*
3D Reconstruction of the Colon from Monocular Sequences: Evaluation by 3D-printed Phantom Data 141

P8 *Leon Weninger, Jarek Ecke, Chuh-Hyoun Na, Kerstin Jütten, Dorit Merhof*
Diffusion MRI Specific Pretraining by Self-supervision on an Auxiliary Dataset 147

P9 *Antonia Popp, Oliver Taubmann, Florian Thamm, Hendrik Ditt, Andreas Maier, Katharina Breininger*
Thrombus Detection in Non-contrast Head CT Using Graph Deep Learning 153

P10 *Christian Matek, Sebastian Krappe, Christian Münzenmayer, Torsten Haferlach, Carsten Marr*
Abstract: A Database and Neural Network for Highly Accurate Classification of Single Bone Marrow Cells 159

P11 *Lukas Burger, Lalith Sharan, Samantha Fischer, Julian Brand, Maximillian Hehl, Gabriele Romano, Matthias Karck, Raffaele De Simone, Ivo Wolf, Sandy Engelhardt*
Comparison of Depth Estimation Setups from Stereo Endoscopy and Optical Tracking for Point Measurements 160

Postersession 2

P12 *Jonas Cordes, Thomas Enzlein, Christian Marsching, Marven Hinze, Sandy Engelhardt, Carsten Hopf, Ivo Wolf*
Abstract: M^2aia: Mass Spectrometry Imaging Applications for Interactive Analysis in MITK 166

P13 *Jan Plier, Matthias Zisler, Jennifer Furkel, Maximilian Knoll, Alexander Marx, Alena Fischer, Kai Polsterer, Mathias H. Konstandin, Stefania Petra*
Learning Features via Transformer Networks for Cardiomyocyte Profiling 167

P14 *Adarsh Bhandary Panambur, Prathmesh Madhu, Andreas Maier*
Effect of Random Histogram Equalization on Breast Calcification Analysis Using Deep Learning 173

P15 *Francesca De Benetti, Verena Bentele, Egon Burian, Marcus Makowski, Nassir Navab, Rickmer Braren, Thomas Wendler*
Longitudinal Analysis of Disease Progression Using Image and Laboratory Data for Covid-19 Patients 179

P16 *Nico Zettler, Derya Dogan, Andre Mastmeyer*
Adipose and Muscular Tissue Removal for Direct Volume Rendering of the Visceral Region in Abdominal 3D CT Images 185

P17 *Ann-Kathrin Greiner-Perth, Eva Marschall, Tobias Kannberg, Benjamin J. Mittmann, Bernd Schmitz, Michael Braun, Alfred M. Franz*
Elektromagnetisches Instrumententracking für die Schlaganfallbehandlung mittels Thrombektomie 191

P18 *Hristina Uzunova, Leonie Basso, Jan Ehrhardt, Heinz Handels*
Abstract: Synthesis of Annotated Pathological Retinal OCT Data with Pathology-Induced Deformations 197

P19 *Sven Koehler, Lalith Sharan, Julian Kuhm, Arman Ghanaat, Jelizaveta Gordejeva, Nike K. Simon, Niko M. Grell, Florian André, Sandy Engelhardt*
Comparison of Evaluation Metrics for Landmark Detection in CMR Images 198

P20 *Marius Pullig, Benjamin Bergner, Amish Doshi, Anja Hennemuth, Zahi A. Fayad, Christoph Lippert*
Deep Learning Models for 3D MRI Brain Classification: A Multisequence Comparison 204

P21 *Lukas Folle, Katharian Tkotz, Fasil Gadjimuradov, Lorenz A. Kapsner, Moritz Fabian, Sebastian Bickelhaupt, David Simon, Arnd Kleyer, Gerhard Krönke, Moritz Zaiß, Armin Nagel, Andreas Maier*
Towards Super-resolution CEST MRI for Visualization of Small Structures 210

P22 *Haobo Song, Chang Liu, Lukas Folle, Andreas Maier*
Multi-organ Segmentation with Partially Annotated Datasets 216

Postersession 3

P23 *Jennifer Furkel, Maximilian Knoll, Shabana Din, Nicolai V. Bogert, Timon Seeger, Norbert Frey, Amir Abdollahi, Hugo A. Katus, Mathias H. Konstandin*
Abstract: C-MORE: A High-content Single-cell Morphology Recognition Methodology for Liquid Biopsies: Toward Personalized Cardiovascular Medicine 222

P24 *Sonja Kunzmann, Christian Marzahl, Felix Denzinger, Christof Bertram, Robert Klopfleisch, Katharina Breininger, Vincent Christlein, Andreas Maier*
First Steps on Gamification of Lung Fluid Cells Annotations in the Flower Domain 223

P25 *Marcin Kopaczka, Lisa Ernst, Mareike Schulz, René Tolba, Dorit Merhof*
Computation of Traveled Distance of Pigs in an Open Field with Fully Convolutional Neural Networks 229

P26 *Laura Graf, Sven Mischkewitz, Lasse Hansen, Mattias P. Heinrich*
Spatiotemporal Attention for Realtime Segmentation of Corrupted Sequential Ultrasound Data: Improving Usability of AI-based Image Guidance 235

P27 *Rebecca Preßler, Kai Lawonn, Bernhard Preim, Monique Meuschke*
Virtual DSA Visualization of Simulated Blood Flow Data in Cerebral Aneurysms 241

P28 *Anselm von Gladiss, Raphael Memmesheimer, Nick Theisen, Anna C. Bakenecker, Thorsten M. Buzug, Dietrich Paulus*
Reconstruction of 1D Images with a Neural Network for Magnetic Particle Imaging 247

P29 *Sonja Jäckle, Tim Eixmann, Florian Matysiak, Malte M. Sieren, Marco Horn, Hinnerk Schulz-Hildebrandt, Gereon Hüttmann, Torben Pätz*
Abstract: 3D Stent Graft Guidance Based on Tracking Systems 253

P30 *Mathias Öttl, Jana Mönius, Christian Marzahl, Matthias Rübner, Carol I. Geppert, Arndt Hartmann, Matthias W. Beckmann, Peter Fasching, Andreas Maier, Ramona Erber, Katharina Breininger*
Superpixel Pre-segmentation of HER2 Slides for Efficient Annotation 254

P31 *Patrick Godau, Lena Maier-Hein*
Abstract: Task Fingerprinting for Meta Learning in Biomedical Image Analysis 260

P32 *Maja Schlereth, Daniel Stromer, Yash Mantri, Jason Tsujimoto, Katharina Breininger, Andreas Maier, Caesar Anderson, Pranav S. Garimella, Jesse V. Jokerst*
Initial Investigations Towards Non-invasive Monitoring of Chronic Wound Healing Using Deep Learning and Ultrasound Imaging 261

P33 *Danilo W. Nunes, Michael Hammer, Simone Hammer, Wibke Uller, Christoph Palm*
Classification of Vascular Malformations Based on T2 STIR Magnetic Resonance Imaging 267

Software Demonstration

S1 *Maximilian Fischer, Philipp Schader, Rickmer Braren, Michael Götz, Alexander Muckenhuber, Wilko Weichert, Peter Schüffler, Jens Kleesiek, Jonas Scherer, Klaus Kades, Klaus Maier-Hein, Marco Nolden*
DICOM Whole Slide Imaging for Computational Pathology Research in Kaapana and the Joint Imaging Platform 273

ePostersession

E1 *Klaus Kades, Jonas Scherer, Jan Scholtyssek, Tobias Penzkofer, Marco Nolden, Klaus Maier-Hein*
Efficient DICOM Image Tagging and Cohort Curation Within Kaapana 279

E2 *Maja Schlereth, Daniel Stromer, Katharina Breininger, Alexandra Wagner, Lina Tan, Andreas Maier, Ferdinand Knieling*
Automatic Classification of Neuromuscular Diseases in Children Using Photoacoustic Imaging 285

E3 *Maximilian Zenk, David Zimmerer, Fabian Isensee, Paul F. Jäger, Jakob Wasserthal, Klaus Maier-Hein*
Realistic Evaluation of FixMatch on Imbalanced Medical Image Classification Tasks 291

E4 *Mehri Baniasadi, Andreas Husch, Daniele Proverbio, Isabel Fernandes Arroteia, Frank Hertel, Jorge Gonçalves*
Initialisation of Deep Brain Stimulation Parameters with Multi-objective Optimisation Using Imaging Data 297

E5 *Sebastian Steindl, Tatyana Ivanovska, Fabian Brunner*
Pathologiespezifische Behandlung von Labelunsicherheit bei der Klassifikation von Thorax-Röntgenbildern 303

E6 *Alexandra Ertl, Alfred Franz, Bernd Schmitz, Michael Braun*
3D CNN-based Identification of Hyperdensities in Cranial Non-contrast CT After Thrombectomy 309

E7 *Annika Niemann, Bernhard Preim, Oliver Beuing, Sylvia Saalfeld*
Predicting Aneurysm Rupture with Deep Learning on 3D Models 315

E8 *Amir El-Ghoussani, Dalia Rodríguez-Salas, Mathias Seuret, Andreas Maier*
GAN-based Augmentation of Mammograms to Improve Breast Lesion Detection 321

E9 *Yuli Wu, Peter Walter, Dorit Merhof*
Multiscale Softmax Cross Entropy for Fovea Localization on Color Fundus Photography 327

E10 *Oliver Aust, Mareike Thies, Daniela Weidner, Fabian Wagner, Sabrina Pechmann, Leonid Mill, Darja Andreev, Ippei Miyagawa, Gerhard Krönke, Silke Christiansen, Stefan Uderhardt, Andreas Maier, Anika Grüneboom*
Tibia Cortical Bone Segmentation in Micro-CT and X-ray Microscopy Data Using a Single Neural Network 333

E11 *Samuel Schüttler, Frederic Madesta, Thomas Rösch, René Werner, Rüdiger Schmitz*
Reinforcement learning-basierte Patchpriorisierung zur beschleunigten Segmentierung von hochauflösenden Endoskopievideodaten 339

E12 *Andreas Maier, Seung Hee Yang, Farhad Maleki, Nikesh Muthukrishnan, Reza Forghani*
Offer Proprietary Algorithms Still Protection of Intellectual Property in the Age of Machine Learning?: A Case Study Using Dual Energy CT Data 345

E13 *Vinothini Selvaraju, Nicolai Spicher, Ramakrishnan Swaminathan, Thomas M. Deserno*
Abstract: Face Detection From In-car Video for Continuous Health Monitoring 351

Unsupervised Segmentation of Wounds in Optical Coherence Tomography Images Using Invariant Information Clustering

Julia Andresen[1], Timo Kepp[1], Michael Wang-Evers[2], Jan Ehrhardt[1,3], Dieter Manstein[2], Heinz Handels[1,3]

[1]Institute of Medical Informatics, University of Lübeck
[2]Cutaneous Biology Research Center, Department of Dermatology, Massachusetts General Hospital, Harvard Medical School
[3]German Research Center for Artificial Intelligence, Lübeck
j.andresen@uni-luebeck.de

Abstract. Monitoring wound healing with optical coherence tomography (OCT) imaging is a promising research field. So far, however, few data and even less manual annotations of OCT wound images are available. To address this problem, a fully unsupervised clustering method based on convolutional neural networks (CNNs) is presented. The CNN takes image patches as input and assigns them to either wound or healthy skin clusters. Network training is based on a new combination of loss functions that require information invariance and locality preservation. No expensive expert annotations are needed. Locality preservation is applied to different levels of the network and shown to improve the segmentation. Promising results are achieved with an average Dice score of 0.809 and an average rand index of 0.871 for the best performing network version.

1 Introduction

The segmentation of anatomical or pathological structures is a crucial step in medical image processing that eases subsequent tasks such as disease monitoring or image registration. Manual segmentation however is time-consuming, error-prone and requires expert knowledge. Automatic segmentation methods such as convolutional neural networks (CNNs) speed up and harmonize medical image segmentation. Still, supervised training of CNNs depends on huge amounts of labelled data which are often not available. In contrast, clustering-based segmentation methods enable the delineation of structures without given labels by grouping similar and separating differing voxels.

In this paper, we present a clustering CNN for the segmentation of wounds in optical coherence tomography (OCT) images of the skin. The network receives image patches as input and assigns them to either wound or healthy skin clusters. Training is based on maximizing the mutual information between network outputs for pairs of original and randomly augmented image patches. This invariant information clustering [1] is combined with a locality-preserving (LP) loss. The LP loss favours similar encodings for close patches which leads to better clustering results. The resulting segmentations are compared to manual delineations of the wound area. Furthermore, we analyze the effect of applying the LP loss at different stages of the network on its clustering abilities.

© Der/die Autor(en), exklusiv lizenziert durch
Springer Fachmedien Wiesbaden GmbH, ein Teil von Springer Nature 2022
K. Maier-Hein et al. (Hrsg.), *Bildverarbeitung für die Medizin 2022*,
Informatik aktuell, https://doi.org/10.1007/978-3-658-36932-3_1

2 Methods

In this section we first delineate the OCT data acquisition and preprocessing procedures. Subsequently, the network architecture and the training scheme for unsupervised wound segmentation are described.

2.1 Data acquisition

We used 12 human skin equivalents (EFT-400, MatTek, Ashland, MA, USA) and induced two circular wounds in the epidermis by a 1.5-mm biopsy punch. The skin equivalents were cultured in medium (EFT-400-ASY, MatTek), and the medium was exchanged daily for one week. An OCT scanner (TEL220C1, Thorlabs) with a central wavelength of 1300 nm was used to acquire volumetric images with an axial resolution of 4.2 μm, a lateral resolution of 13 μm (LSM03, Thorlabs), and a dimension of $3\times3\times3.5\,\text{mm}^3$ (spatial FOV: $461\times461\times1024$ voxels). OCT images were taken on day 0, 1, 2, 3, 4 and 7 after the epidermal injury for each wound separately leading to 144 images in total.

2.2 Preprocessing

Due to poor contrast and large image size we perform average-smoothing on each horizontal slice and reduce the resolution to $64\times128\times284$ voxels. In a second step a flattening of the upper skin border is performed as shown in Figure 1. To do so, we 1) calculate the image gradient magnitude, 2) A-scan-wise extract the maximum gradient and enter its position into a height map, 3) mask the central area of the height map, 4) smooth the height map, 5) fill the masked area using bilinear interpolation and 6) translate each A-scan according to the height map so that the maximum gradient position is shifted to a fixed slice. The rectangular-shaped mask used in step 3) is selected by manual inspection and covers all wounds entirely. Like this, the translation of A-scans is based only on the position of the intact skin. Finally, the images are cropped to the upper $64\times128\times92$ voxels.

2.3 Clustering network

The architecture of the network is depicted in Figure 2. It consists of a convolutional backbone and two clustering heads each composed of three fully-connected (FC) layers

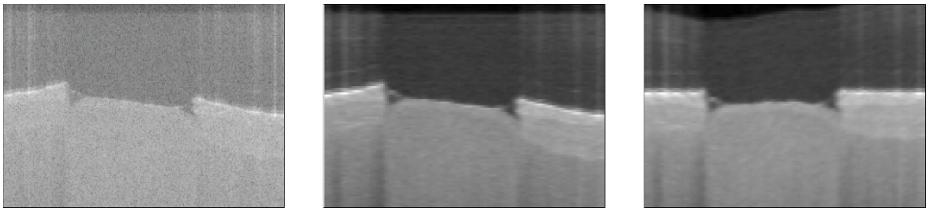

Fig. 1. Preprocessing steps taken before clustering. Left: original, middle: smoothing and down-sampling, right: flattening.

and a final softmax activation. Input to our clustering network are 3D patches of size $11 \times 11 \times 92$ voxels. The output of the convolutional backbone is flattened and concatenated with a vector indicating the patch position in the image volume. The enlarged feature vector then serves as input to the first FC layers of main and overclustering head. The main head outputs a two-entry vector that contains the probabilities of the patch belonging to the wound and healthy skin clusters while the overclustering head produces ten instead of two clusters. Both heads are trained simultaneously with the same loss function allowing the overclustering head to discriminate patches inside the same cluster while maintaining the skin and wound predictions of the main head. This may help to increase expressivity in the learned features [1, 2].

2.4 Loss functions

The network $\Phi(\theta)$ with its corresponding parameters θ is trained using a two-component loss function based on invariant information clustering (IIC) and locality preservation. The objective of IIC is to maintain similarities between paired inputs and to discard instance-specific details. This is achieved by maximizing the mutual information between the soft clustering outputs of the paired inputs [1]. To use IIC for wound segmentation we apply this principle on pairs of image patches. Each pair consists of one original image patch $\boldsymbol{x}$ and a randomly augmented version $\boldsymbol{x}'$ of this patch. Augmentation includes the addition of random noise and random intensity transformations. The IIC part of the loss function is then given by

$$\mathcal{L}_{\mathrm{IIC}}(\theta; \boldsymbol{x}, \boldsymbol{x}') = -\mathrm{MI}\big(\Phi(\theta; \boldsymbol{x}),\ \Phi(\theta; \boldsymbol{x}')\big) \tag{1}$$

which has the effect of discarding differences between augmented and original patch and of making the network outputs the same for both patch versions.

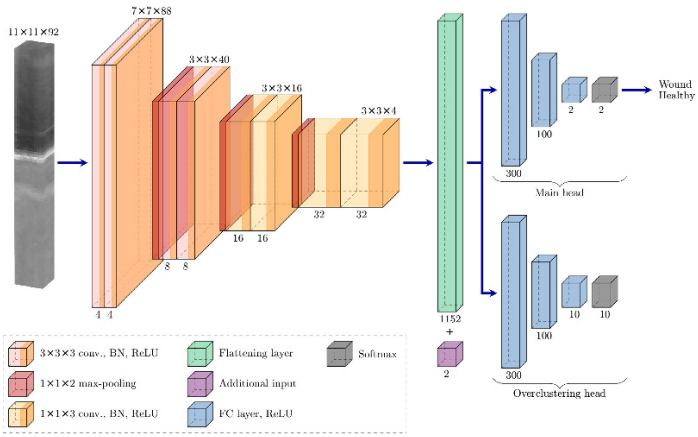

Fig. 2. Architecture of the patch-wise clustering network for wound segmentation. A convolutional backbone is followed by three FC layers. No padding is performed in the convolutional layers. Numbers below the convolutional layers indicate number of feature maps while the numbers above give the size of the outputs of the last convolutional layer.

To prevent inhomogeneous clusters, we add a second term to the loss function. The LP loss takes two patches $\boldsymbol{x}_i$ and $\boldsymbol{x}_j$ of the same image volume as input and favours similar encoded representations z_i and z_j for close patches. Inspired by [3, 4] we define

$$\mathcal{L}_{\mathrm{LP}}(\theta; \boldsymbol{x}_i, \boldsymbol{x}_j) = \omega\big(\|\boldsymbol{l}_i - \boldsymbol{l}_j\|_2\big) \cdot \mathrm{s}(\boldsymbol{x}_i, \boldsymbol{x}_j) \cdot \|z_i - z_j\|_2^2 \tag{2}$$

Here, $\boldsymbol{l}_i$ is the location of patch $\boldsymbol{x}_i$, s is an image similarity measure and ω a weighting function assigning small distances a large weight and setting large distances to zero. Like this, spatially close patches are pushed to similar encodings while distant patches may be clustered independently. The final loss function is calculated for all consecutive patch pairs in a batch and defined by

$$\mathcal{L}(\theta; \boldsymbol{x}_i, \boldsymbol{x}_j) = \mathcal{L}_{\mathrm{IIC}}(\boldsymbol{x}_i, \boldsymbol{x}_i') + \mathcal{L}_{\mathrm{IIC}}(\boldsymbol{x}_j, \boldsymbol{x}_j') + \mathcal{L}_{\mathrm{LP}}(\boldsymbol{x}_i, \boldsymbol{x}_j) + \mathcal{L}_{\mathrm{LP}}(\boldsymbol{x}_i', \boldsymbol{x}_j') \tag{3}$$

The network is trained for 200 epochs, with Adam optimization and an initial learning rate of $1\mathrm{e}^{-6}$. For each epoch, 150 pairs of patches per volume are drawn at random using a uniform distribution and passed through the network. During inference only original image patches (rather than pairs of patches) are input to the network and the overclustering head is ignored. The main head's clustering result is kept for the patch's central A-scan that is assigned the cluster with highest probability to achieve an A-scan-wise segmentation result.

3 Results

For evaluation, a six-fold cross-validation is performed, training the network on 120 images of 10 skin equivalents and testing it on the remaining 24 images. For each test set one of the four included wounds is manually segmented over all time points. The clustering ability of the networks is checked quantitatively comparing results to the manual segmentations and qualitatively using t-distributed stochastic neighbor embedding (t-SNE) for visualization [5].

We train several versions of our clustering method applying the LP loss on different levels of the network. Successively, the feature vectors output by convolutional backbone, first, second and third FC layer are used as encoded representations z in equation (3). Note that applying the LP loss on the network output is similar to the local spatial invariance used in [1]. Network versions are denoted with LP-Conv, LP-FC1, LP-FC2 and LP-FC3, respectively, and we report average DSC and rand index (RI) compared to the manual labels in Table 1. Additionally, results are reported for training without applying the LP loss (IIC only).

Results show that the clustering network learns to well distinguish between patches lying inside or outside of the wound. The LP loss greatly improves performance compared to the network trained on IIC alone leading to an average DSC of 0.809 for LP-Conv. For this best performing network version exemplar segmentation results are displayed in Figure 3 which shows that even the segmentation of the image with lowest DSC is still close to the actual wound area. Although the flattening does not work for this image because of the partially detached epidermis, the CNN still produces useful results.

Tab. 1. Results of the clustering network trained by applying LP on different levels. Average DSC and RI are reported. In brackets the minimal and maximal values are given and best results are presented in bold font.

Method	DSC	RI
IIC only	0.464 (0.339, 0.655)	0.479 (0.254, 0.743)
LP-Conv	**0.809** (0.678, 0.960)	**0.871** (0.768, 0.981)
LP-FC1	0.761 (0.596, 0.892)	0.832 (0.676, 0.939)
LP-FC2	0.777 (0.648, 0.914)	0.845 (0.743, 0.955)
LP-FC3	0.494 (0.312, 0.649)	0.607 (0.347, 0.779)

To further analyze the effect of the LP loss on the clustering abilities of the network, principle component analysis is used to reduce the high-dimensional feature vectors of convolutional backbone, first and second FC layer to a size of 50. Afterwards t-SNE plots are generated to visualize features in two dimensions (perplexity set to 50, further experiments with different values led to similar results). Plots are generated with 850 randomly selected patches per skin equivalent in the first test set. Representative results in Figure 4 show that especially for LP-FC1 and LP-FC2 the separability of clusters is increased in the feature space the LP loss is applied in. Also it can be seen that using the LP loss leads to clusters aligning well with wound and healthy skin whereas IIC only generates more intertwined clusters. This reflects the quantitive results showing how the LP loss helps to generate better segmentation results compared to training with IIC only.

4 Discussion

In this paper, a method for unsupervised segmentation of OCT wound images is presented. Without using any labelled data, the clustering network learns to distinguish

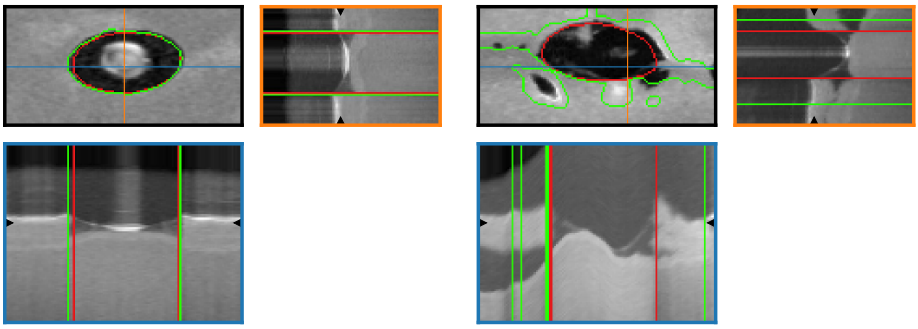

(a) DSC of 0.960 (A1, day 0) **(b)** DSC of 0.678 (E1, day 1)

Fig. 3. Segmentation results on best (a) and worst (b) performing test images compared to manual ground truth. Predicted and ground-truth segmentation contours are shown in green and red, respectively. Black triangles, blue and orange lines mark the position of the other depicted image slices.

Fig. 4. T-SNE plots displaying the feature vectors of convolutional backbone (1st and 4th columns), first (2nd and 5th columns) and second FC layer (3rd and 6th columns) in two dimensions for IIC only (a, b, c), LP-Conv (d, e, f), LP-FC1 (g, h, i) and LP-FC2 (j, k, l).

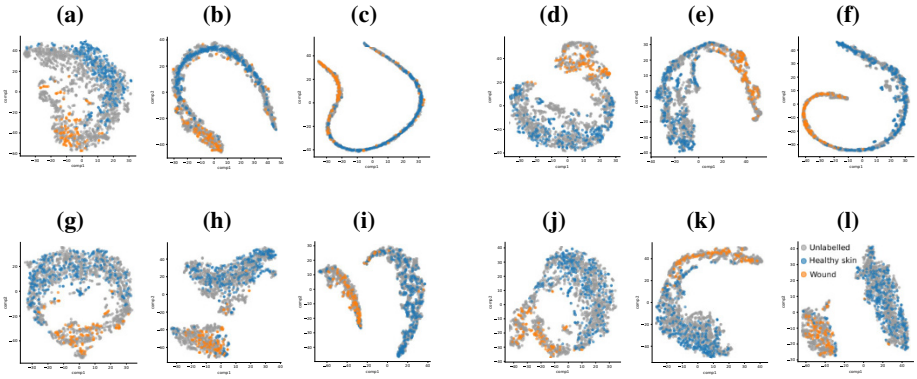

patches lying outside or inside of the wound. T-SNE plots show that the LP loss helps to form better separable clusters in the feature space leading to good segmentation results. Best results are achieved using the outputs of the convolutional backbone to calculate the LP loss with a mean Dice score of 0.809 compared to manually segmented images.

Still, further investigations on the best choice of hyperparameters and a more sophisticated quantitative evaluation of the method need to be done. We plan to analyze the effect of different patch sizes. The network tends to oversegment the wound area which we assign to the relatively large patch size. Smaller patch sizes down to A-scans might help prevent this problem. Moreover, we intend to test the clustering network for unsupervised segmentation of retinal OCT images.

All in all, our clustering network is a promising method for unsupervised detection and segmentation of pathologies in medical images. It is not limited to OCT images and may also be used to segment anatomical structures. Since no manual labels are required for network training the method is applicable to a wide range of datasets.

References

1. Ji X, Henriques JF, Vedaldi A. Invariant information clustering for unsupervised image classification and segmentation. Proc IEEE ICCV. 2019:9865–74.
2. Do K, Tran T, Venkatesh S. Clustering by maximizing mutual information across views. Proc IEEE ICCV. 2021:9928–38.
3. Aljalbout E, Golkov V, Siddiqui Y, Strobel M, Cremers D. Clustering with deep learning: taxonomy and new methods. arXiv preprint. 2018;arXiv:1801.07648.
4. Huang P, Huang Y, Wang W, Wang L. Deep embedding network for clustering. Proc IEEE ICRR. 2014:1532–7.
5. Van der Maaten L, Hinton G. Visualizing data using t-SNE. J Mach Learn Res. 2008;9(11):2579–605.

Iterative 3D CNN Based Segmentation of Vascular Trees in Liver CT

Mona Schumacher[1,2], Ragnar Bade[2], Andreas Genz[2], Mattias Heinrich[1]

[1]Institute of Medical Informatics, Lübeck University
[2]MeVis Medical Solutions AG, Bremen
mona.schumacher@mevis.de

Abstract. The segmentation of vascular systems is a challenging task since their sizes and structures vary greatly so that the spatial context becomes highly important. For further clinical analysis of the vascular system it is important to create a connected vascular tree starting from the main trunk, following the tree structure up to small branches. To address these issues, we propose a new iterative segmentation model that recursively evolves a segmentation of a vasculature by following its tree structure. Our iterative CNN alternates between three steps: First, a 3D segmentation of a sub-region is performed. Second, branches that are not part of the currently analyzed branch are removed and third, subsequent sub-regions are detected. These steps are repeated until the entire vascular system is segmented. We trained, validated and tested our model on 82 CT images. We showed that, in comparison to state of the art methods, our new model generates a more accurate segmentation, resulting in an improvement of the Dice score of 7 % and a reduction of the Hausdorff distance of approximately 20 %.

1 Introduction

Different clinical workflows require a precise segmentation of the vessels in the liver, e.g. for tumor resections. For these clinical applications, the correct detection of both small and large vessel structures is as important as the vessel tree connectivity and topology [1]. However, due to the low contrast between the vessels and surrounding liver parenchyma as well as the high complexity of the branching structures of the vessel systems, the segmentation is known to be a challenging task. In addition, the contrast between vessels and liver parenchyma can vary across CT scans since the timing of the acquisition is very important.

Deep learning methods for segmentation are less dependent and more robust against gray values and image quality. Popular architectures for the segmentation of structures are the U-Net [2] or variants of it [3, 4]. However, due to the size of the contrast enhanced CT input scan, the images often need to be downsampled or trained with a patch-based approach, because they cannot be processed at once due to the limited GPU memory. In the area of vascular segmentation this means, that small veins could possibly not be detected anymore because they would be removed during downsampling. Furthermore,

© Der/die Autor(en), exklusiv lizenziert durch
Springer Fachmedien Wiesbaden GmbH, ein Teil von Springer Nature 2022
K. Maier-Hein et al. (Hrsg.), *Bildverarbeitung für die Medizin 2022*,
Informatik aktuell, https://doi.org/10.1007/978-3-658-36932-3_2

the available 3D deep learning approaches also do not detect the tree topology correctly, which results in a segmentation with several unconnected components.

Due to the importance of parameter optimization, preprocessing, and data augmentation of the images that have a great influence on the performance of the network, the nnU-Net, introduced by Isensee et al. [5], has gained significant impact since its publication in 2019 and can currently be regarded as the state of the art method for medical image segmentation. However, even this approach does not generate a vessel segmentation with a continuous, connected tree structure that is important to analyze the blood flow and the supply of the remaining liver tissue.

1.1 Contributions

This paper presents a new iterative patch-based method to segment vessel trees from medical imaging data. Our proposed method overcomes the issues of currently available segmentation methods, and detect a continuous tree including small branches, and is able to cover the complex tree structure of the vessels. Starting from a manually selected seed, our method subsequently segments vascular trees in a 3D sub-region and detects the next regions of interest (ROI) depending on the course of the vessel and the number of branches in the segmented region until the entire vascular system is segmented.

2 Materials and methods

For training and evaluation of our method, a dataset of 82 contrast enhanced liver CT images of the venous phase from different centers and scanners with an image extend in a range of $313 \times 22 \times 86$ to $510 \times 421 \times 413$ voxels with voxel sizes of $0.39 \times 0.39 \times 0.97$ to $0.97 \times 0.97 \times 3.0$ mm are used.

Images are either acquired to plan a living liver donation (healthy patients) or a tumor resection. The dataset thus includes both images of healthy and diseased patients.

When acquiring contrast enhanced CT images, the timing is not always ideal in respect to the contrast enhancement of the vascular system to the surrounding structures. Our dataset shows a variety of contrasts in or outside of the portal vein, so that images with well contrasted (high gray values) as well as poorly contrasted portals veins (lower gray values, more similar to liver parenchyma) are included, which results in high variety of gray values of the portal vein.

For all of these images, ground truth labels are available. The data has been manually segmented and reviewed by three experienced radiologic technicians. The remarkable aspect of these annotations is that very small vessels are also included in the segmentation. Moreover, the resulting vascular tree is one connected component that can be used to analyze the blood supply of the liver parenchyma which is important to plan a liver surgery.

We clamped the image value range from 0 to 700 HU. The normalization of the images is done by subtracting the mean (170.81 HU) followed by a division by the standard deviation (36.70 HU) of the HU values within the portal vein of our training images and scale the image values from 0 to 1 afterwards. We do not resample our input data to a uniform voxel size to emphasize that vessel branches can be of different sizes.

Finally, we split the data for all experiments in a training, validation and testing set of 40, 10 and 32 image pairs, respectively.

To solve the issues described above, our model iteratively segments the vessels by following its tree structure. Starting from a manually selected seed point, the portal vein is segmented in a given sub-region with a 3D U-Net. Based on the segmentation in the sub-region, the next sub-region(s) are identified to follow the course of the vessels in consideration of the branching structure. The iterative segmentation stops if no new sub-regions are identified. An overview of the segmentation pipeline is shown in Figure 1. We start with a CT scan and an vessel tree result image in iteration step $i = 0$. The result image is accumulated with values at each iteration step to get the final segmentation. The queue is processed according to the FIFO (first-in-first-out) principle.

To demonstrate the beneficial effect of the removal of components from other vessel branches, we additionally evaluate our described iterative approach without the removal of these components (WithoutRemoval).

In addition, we train the 3D full resolution nnU-Net (3DnnU-Net), as described in [5] and a standard sliding window approach with a patch size of $128 \times 128 \times 64$ and an overlap of 50 %. To get a connected vascular tree, we perform a connected component analysis and keep the largest component to get the final segmentation result.

In the following, our method is described in more detail.

2.1 Segmentation of sub-regions

The segmentation of the sub-regions is done with a 3D U-Net. We train our model with two different patch sizes: $64 \times 64 \times 64$ (OursSmall) and $128 \times 128 \times 64$ (OursLarge).

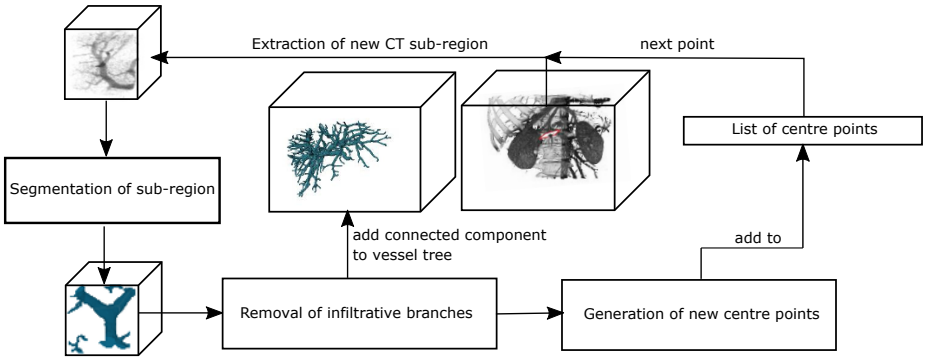

Fig. 1. Pipeline of proposed vessel segmentation method: Starting from a selected seed point, a 3D sub-region around the seed point is segmented with a U-Net. To contiguously track the vascular tree, connected branches in the segmented sub region are kept (components from other branches are removed) and new seed points for further tracking are detected. Such new seed points will be generated at the faces of the current cubical sub-region depending on the current tracking path and the number of tree branches in the segmented sub-region. Thus, iteratively the vascular tree is built up further until no new seed points are detected.